PRAMANA — journal of physics

Vol. 81, No. 2
August 2013
pp. 331–341

Preparation and investigation of optical, structural, and morphological properties of nanostructured ZnO:Mn thin films

E AMOUPOUR[1,*], F E GHODSI[2], H ANDARVA[2] and A ABDOLAHZADEH ZIABARI[3]

[1]Department of Electronic Engineering, Roudsar & Amlash Branch, Islamic Azad University, Roudsar, Iran
[2]Department of Physics, Faculty of Science, University of Guilan, Namjoo Avenue, P.O. Box 413351914, Rasht, Iran
[3]Department of Physics, Faculty of Science, Lahijan Branch, Islamic Azad University, P.O. Box 1616, Lahijan, Iran
*Corresponding author. E-mail: Amoupour@yahoo.com

MS received 17 January 2013; revised 7 April 2013; accepted 17 April 2013

Abstract. Nanostructured ZnO:Mn thin films have been prepared by sol–gel dip coating method. The content of Mn in the sol was varied from 0 to 12 wt%. The effect of Mn concentration on the optical, structural, and morphological properties of ZnO thin films were studied by using Fourier transform infrared (FTIR), UV–visible and photoluminescence (PL) spectroscopy, X-ray diffraction (XRD) and scanning electron microscopy (SEM). XRD results showed that the films have hexagonal wurtzite structure at lower content of Mn. The diffraction peaks corresponding to ZnO disappeared and two diffraction peaks of MnO_2 and Mn_3O_4 appeared at the highest value of doping concentration (viz., 12 wt%). SEM results revealed that the surface smoothness of the films improved at higher content of Mn. The optical band gap of the films decreased from 3.89 to 3.15 eV when the Mn concentration increased from 0 to 12 wt%. The PL spectra of the films showed the characteristic peaks linked to band-to-band, green and yellow emissions. Besides, the PL intensity of the samples decreased with increase in Mn concentration.

Keywords. ZnO:Mn; nanocrystalline thin film; sol–gel; optical properties.

PACS Nos 81; 78.20.–e; 78

1. Introduction

The preparation and study of nanocrystalline semiconductors are of significant interest due to their tunable electronic, optical, and catalytic properties arising from the size confinement effect [1,2]. Especially, group II–VI compound semiconductors have drawn

much attention due to their several advantages [3]. Because of its unique electrical, optical, and piezoelectric properties, ZnO has been used in a number of devices [4,5]. ZnO is considered as a significant optoelectronic device material for use in the blue and violet regions because of its wide band gap (∼3.37 eV). Moreover, due to its piezoelectric properties, ZnO thin films have widely been used in the surface-acoustic wave (SAW) devices [6]. Ordered *c*-axis orientation of ZnO crystallites is desirable for applications where crystallographic anisotropy is a prerequisite for piezoelectric surface-acoustic wave or acousto-optic devices [7]. ZnO nanostructures find applications in short-wavelength light-emitting diodes [8], field-emission devices [9], solar cells [10], and sensors [11].

There are several reports on the preparation of ZnO thin films by different methods such as pulsed laser deposition [12], RF magnetron sputtering [13], chemical vapour deposition (CVD) [14], molecular beam epitaxy (MBE) [15], spray pyrolysis [16], etc. However, only a few reports are available on the optical behaviour of Mn-doped ZnO thin films prepared by chemical sol–gel process [17,18]. Sol–gel dip-coating is a thin film deposition technique that has many benefits, such as easier composition control, better homogeneity, and lower cost [19]. ZnO is an n-type semiconductor and the electrical conductivity of the undoped ZnO thin films is mainly due to either the oxygen vacancy or the presence of interstitial Zn in ZnO lattice [20]. The resistivity of ZnO thin films depends largely on the type of doping and preparation technique and can be varied from 10^{-4} to 10^{10} Ω cm. The nature of the doping material may affect the electronegativity because of the different ionic radius between Zn and the doping element. So far, many reports are available on ZnO being doped with In, Al, Ga, P, N, Li, Mg, etc. for improving its electrical and optical properties [21,22]. Some articles on Mn-doped ZnO films have concentrated on the ferromagnetic properties [23,24].

These suggest that, regardless of the methods of preparation, ZnO possesses a great potential to be treated more fundamentally. Particularly, the possible correlation between the physical characteristics like structural, morphological, and optical features is still an open problem. As a transition metal, Mn would be a proper candidate to tune the band gap and also control the growth rate of the nanograins.

In the present work, we try to conduct an investigation on the effects of Mn doping on the structural, morphological, optical, and photoluminescence properties of ZnO thin films and study the probable correlation between them.

2. Experimental details

Using sol–gel dip-coating method, Mn-doped ZnO thin films were deposited onto a glass substrate. Before deposition, the substrates were carefully washed with a detergent and then rinsed by distilled water and cleaned with acetone by an ultrasonic cleaner.

The starting solution was synthesized using zinc acetate dihydrate ($Zn(CH_3COO)_2{\cdot}2H_2O$) as the source of Zn, 2-propanol (0.6 M) as the solvent and diethanolamine ([DEA]/$[Zn^{2+}] = 1$) as the stabilizer. Initially, zinc acetate dihydrate was dissolved in 2-propanol and the obtained mixture was heated and stirred for 1 h using a magnetic stirrer. Then, manganese acetate tetrahydrate was added to the solution as the Mn source to prepare thin films of various concentrations of Mn doping (0, 1, 3, 5, 8 and 12 wt%). Finally, the sol was heated and stirred for 1 h. The withdrawn speed (the speed that the coated substrate is

pulled up) was kept at 9 cm/min. After each deposition, all samples were dried at 210°C for 20 min to remove the solvent and organic residuals. Finally, the films were annealed at 450°C for 60 min in air ambient. Also, the drop-casted films were prepared at the same condition with higher thickness.

The optical transmission spectra of Mn-doped ZnO thin films were measured using a Varian Cary100 UV–vis spectrophotometer. The optical constants of the films were determined using point-wise unconstrained minimization approach (PUMA) and fitting the data to the Cauchy formula for thin films [25]. Infrared spectrum of the samples was measured by using Fourier transform infrared (FTIR) spectrophotometer (Bruker model Vertex 70) for identifying the molecular composition. An analysis of the crystalline structure and the texture of the films were performed by a Philips PW-1840 diffractometer using Cu K_α radiation ($\lambda = 0.154$ nm). The surface morphology of the films was investigated by SEM (Philips, XL30) with 15 kV accelerating voltage. The photoluminescence spectra of the films were examined by Perkin Elmer (LS 55) fluorescence spectrometer under excitation at 297 nm.

3. Results and discussion

XRD patterns of the undoped and Mn-doped ZnO thin films are shown in figure 1. As can be seen from figure 1, there are three peaks for the bare ZnO which is identified as having the wurtzite structure. The peaks corresponding to this structure in this pattern are (1 0 0), (0 0 2), and (1 0 1) appearing at 2θ values of 31.82°, 34.47°, and 36.74°, respectively. On the other hand, when Mn concentration increases, the intensity of the peak decreases. It can also be observed that the characteristic peaks of ZnO disappear as Mn incorporation

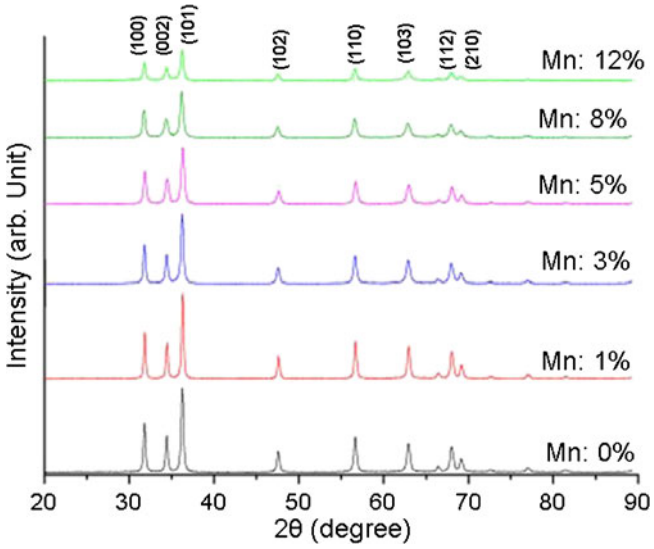

Figure 1. XRD patterns of ZnO:Mn thin films at 0, 1, 3, 5, 8 and 12 wt% Mn concentrations.

reaches 12 wt% and two diffraction peaks corresponding to MnO_2 and Mn_3O_4 phases with (2 1 1) and (2 2 0) planes around 38.25° and 44.43° [26,27] appear. Due to the low thickness of the films, to ensure the reliability of the peaks of XRD patterns, the drop-casted films were prepared just under the same condition of the ordinary films. It was revealed that the peak intensity enhanced drastically for the drop-casted films in comparison with dip-coated ones. Moreover, additional peaks of ZnO appear while the diffraction peaks of MnO_2 and Mn_3O_4 disappear because of their lower intensity compared to ZnO peaks.

The grain size of the films was calculated by Scherer's formula [28] and the results are given in table 1. Overall, the grain size decreases with Mn concentration. The lattice parameters were obtained by the following equations [29]:

$$a = \sqrt{\frac{1}{3}}\frac{\lambda}{\sin\theta}, \tag{1}$$

$$c = \frac{\lambda}{\sin\theta}. \tag{2}$$

The corresponding values for the bulk material are $a_0 = 3.25$ Å and $c_0 = 5.21$ Å.

The scanning electron microscopy (SEM) was used to study the morphology of the present ZnO:Mn thin films. Figure 2 illustrates the micrographs of the nanostructured ZnO:Mn thin films prepared by sol–gel dip-coating method. The SEM image taken from bare ZnO shows a granular pattern with spherical shapes distributed within it. This type of surface morphology was observed for samples with different Mn content. However, when Mn content increases, the size of granules decreases and the surface of the film shows smoother morphology. As shown in figure 2f, the granular size of ZnO thin films with 12 wt% of Mn content is very small and cannot be distinguished well by the present SEM micrographs. These results confirm that introducing manganese hinder the growth of granules as reported in [30,31].

To prepare samples for FTIR analysis, first the prepared sol was strewed on the surface of the substrate and then the heat treatment that was explained for the ordinary samples was given. Afterwards, freestanding thick films were obtained by scratching the surface

Table 1. The calculated grain and lattice parameters for nanostructured ZnO:Mn thin films.

Mn Content	Grain size (nm)	Lattice parameters (Å)	
		a	*c*
Undoped ZnO	18	3.03	5.26
1%	18	3.03	5.26
3%	17	3.03	5.26
5%	16	3.02	5.24
8%	15	2.70	4.69
12%	12	2.71	4.70

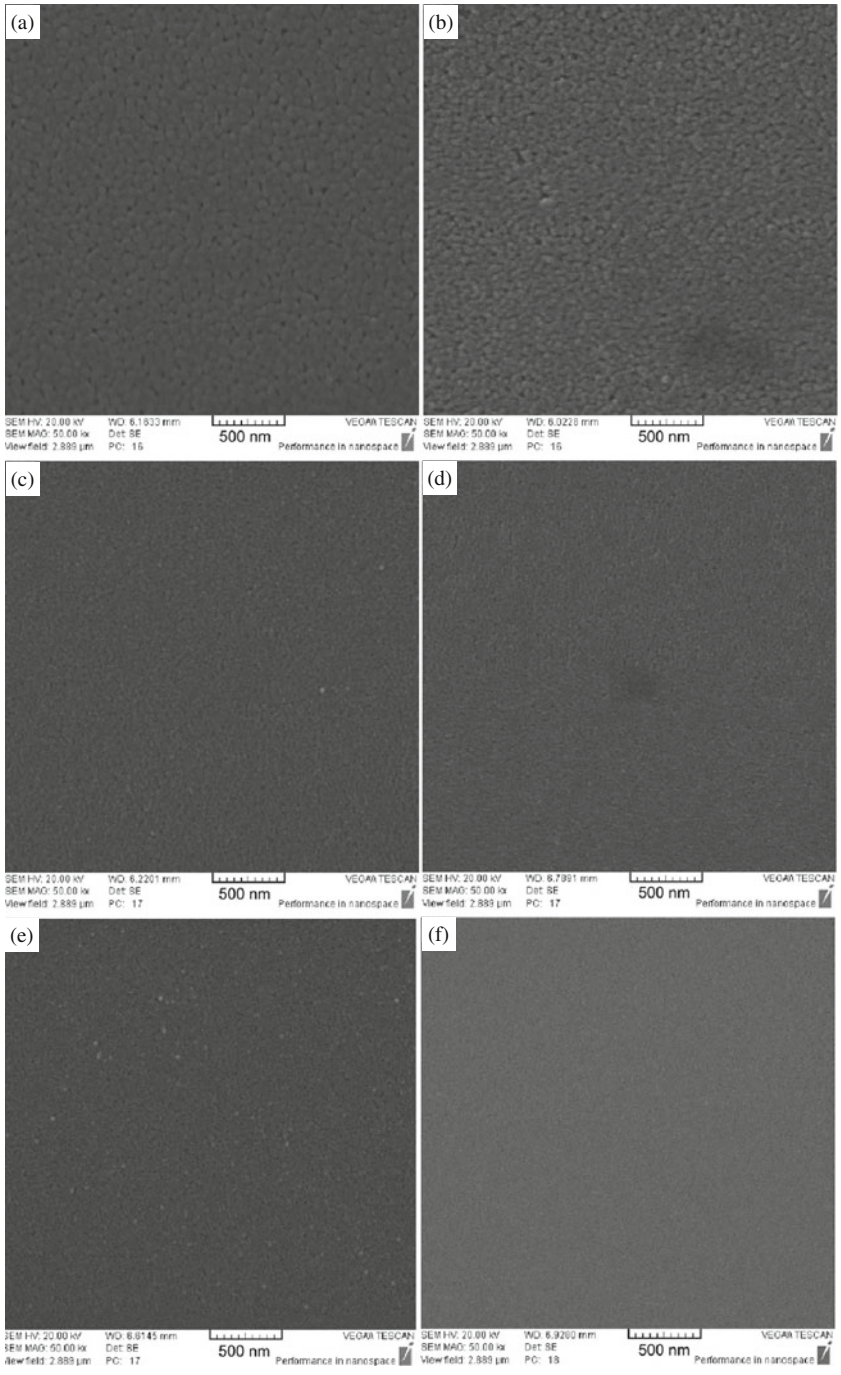

Figure 2. SEM micrographs of nanostructured ZnO:Mn thin films at various Mn concentrations, (**a**) undoped, (**b**) 1 wt%, (**c**) 3 wt%, (**d**) 5 wt%, (**e**) 8 wt%, and (**f**) 12 wt%.

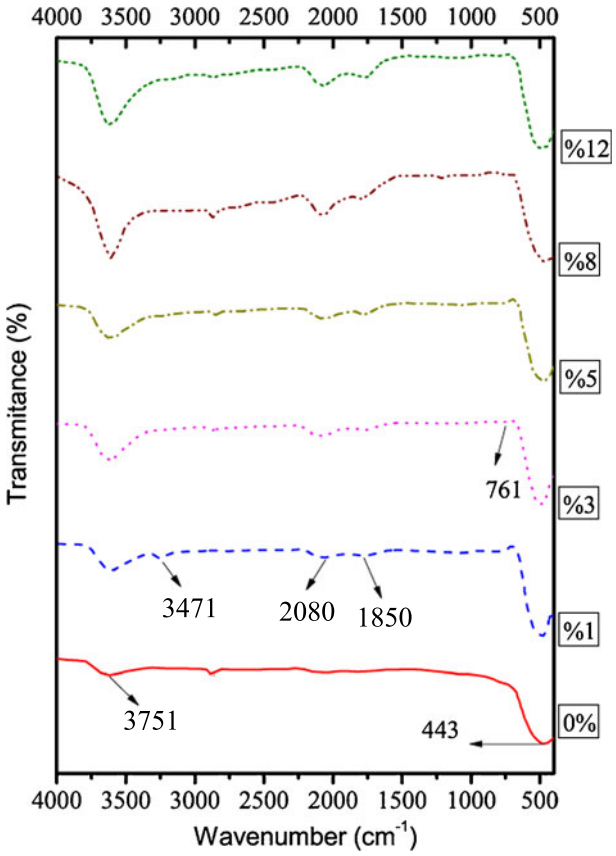

Figure 3. FTIR spectra of Mn-doped ZnO at 0, 1, 3, 5, 8, and 12 wt% Mn doping concentrations.

of the substrate. Finally, KBr pellets were prepared from different wt% of Mn-doped ZnO powders, and the spectrum was measured.

The FTIR spectra of the pure ZnO indicate three peaks (figure 3). The broad peak around 3471 cm^{-1} or should be absorbed water in acetates [32]. The band at ∼3751 cm^{-1} is related to the N–H vibration mode related to DEA (as the stabilizer). The intensity of the peaks increases as the concentration of Mn increases. Additionally, two broad peaks gradually emerge as the concentration of Mn increases. These peaks are observed at ∼1850 cm^{-1} and ∼2085 cm^{-1} and can be assigned to the asymmetric and symmetric C=O stretching mode of acetate groups [33]. It seems that with increasing Mn concentration, the concentration of acetate ion (CH_3COO^-) increases. The most important change is the formation of a peak below 443 cm^{-1}, that may be due to the Zn–O and (Zn–Mn)–O stretching modes [33]. A peak with low intensity at ∼761 cm^{-1} can be ascribed to the ZnO stretching mode, as reported in [34].

The spectral behaviour of transmittance in the range of 200 to 800 nm for ZnO:Mn thin films are shown in figure 4. The figure shows an average optical transparency between 80

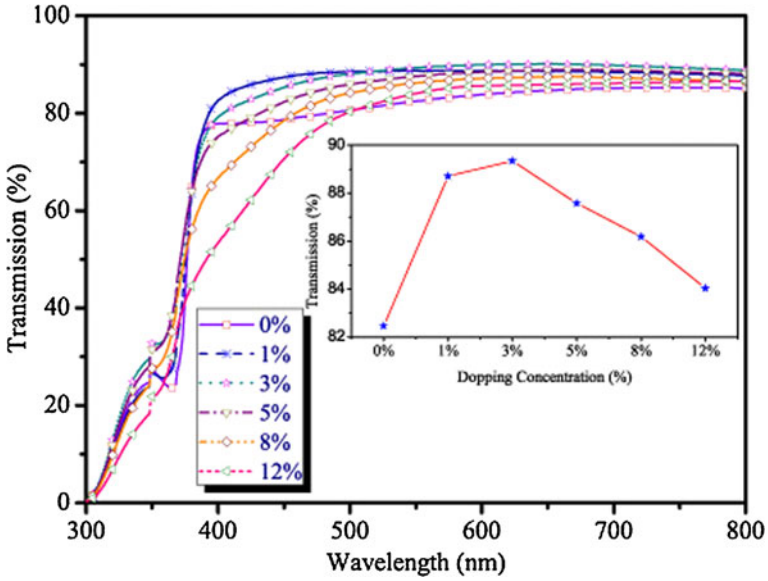

Figure 4. The transmission spectra of the Mn-doped ZnO thin films vs. wavelength.

and 90% in the visible region of the spectrum. Obviously, with increasing Mn concentration in ZnO:Mn thin films, the transmittance increases tardily until it reaches its highest value (viz. 89% for 3 wt% of Mn). However, with increasing doping percentage up to 12 wt%, the transmittance reduces to 84%. Another aspect of the measured transmittance spectra is that the absorption edge of the films will be shifted to shorter wavelengths with doping up to 3 wt% of Mn and then shifted to longer wavelengths for higher levels of doping. To examine this assumption, we calculated the band gap value of the samples by means of optical data and the well-known Tauc formula (figure 5 and table 2). Clearly, in coincidence with transmittance spectrum, the maximum/minimum band gap belongs to the sample with 1 wt%/12 wt% of Mn content.

Another thing that seems noteworthy in the optical transmission spectra of undoped, 1 wt%, 3 wt% and 5 wt% doped samples, is a shoulder at lower wavelengths in the vicinity of optical edge. This may be related to the Urbach tail that usually extends into the band edge due to some thermal/static structural disorder and impurities in thin films [35]. The optical band gap, refractive index, and thickness of ZnO:Mn thin films with various concentrations of Mn are given in table 2. By introducing dopants, many of the characteristics of a semiconductor would change due to either high concentration of impurities or high carrier concentration. These factors may induce some effects such as Mott transition, the Burstein–Moss shift, band-tailing effects, and band-gap renormalization [36]. With Mn^{2+} incorporation up to 1 wt%, the band-gap value enhances which then decreases suddenly for higher Mn concentrations. The sudden increase in the band gap with Mn may be due to the well-known Burstein–Moss effect though it is a fact that the band gap of MnO (4.2 eV) is larger than ZnO (3.2 eV). Hence, the decrease in band gap at higher doping concentration can be a consequence of band gap narrowing or band gap renormalization as explained elsewhere [4,37,38].

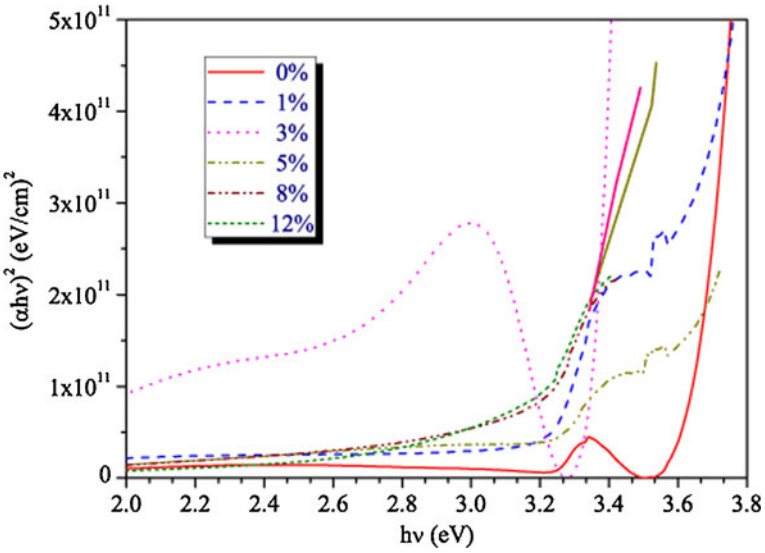

Figure 5. The plots of $(\alpha h\upsilon)^2$ vs. photon energy of nanstructured ZnO:Mn thin films.

Figure 6 shows the room-temperature PL spectra of the nanocrystalline ZnO thin films with different Mn concentrations. As it is obvious from figure 6, the PL intensity decreases with increase in Mn concentration that might be attributed to the occurrence of some non-radiative recombination processes during Mn doping [39]. The UV emission, centred at ∼376 nm, is attributed to the near band edge (NBE) free excitation transitions which can happen even at room temperature for ZnO. The peak around 400 nm (3.10 eV) is very intense and the origin of the corresponding emission is not clear so far [40]. It is probably caused by the electron transition from the energy level of interstitial Zn to valance band [41,42]. The appearance of 400 nm peak probably implies the existence of Zn interstitials in these sol–gel-derived ZnO nanostructured thin films [43]. The high intensity of 400 nm peak in the undoped ZnO film suggests that a large amount of interstitial Zn may be present in the mentioned case. Also, the peak at 489 nm is related to the transition from energy level of singly ionized interstitial zinc (Zn_i) to local zinc vacancy

Table 2. The band-gap energy, refractive index, and film thickness of nanostructured ZnO:Mn thin films prepared by sol–gel.

Mn Content	Band Gap (eV)	Refractive index ($\lambda = 550$ nm)	Film thickness (nm)
0%	3.89	1.73	155
1%	3.90	1.71	145
3%	3.84	1.60	110
5%	3.82	1.70	165
8%	3.20	1.73	140
12%	3.15	1.78	140

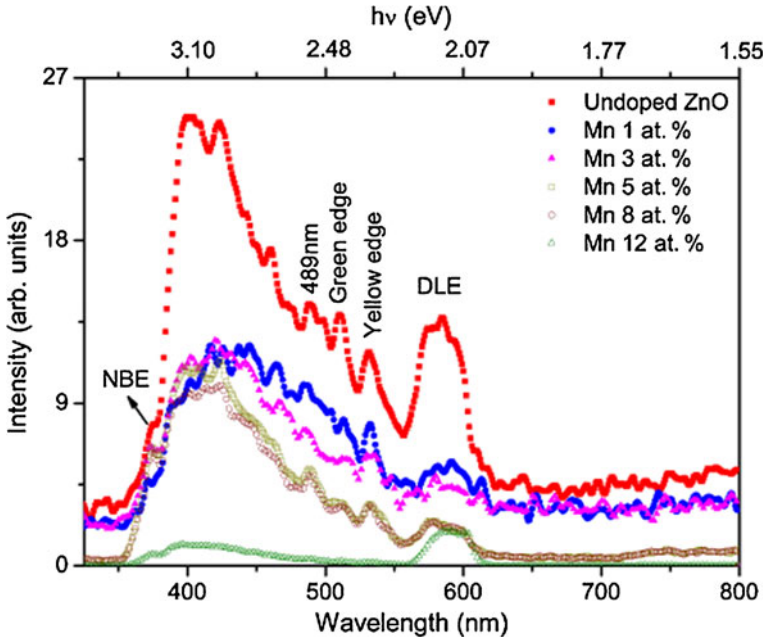

Figure 6. Photoluminescence (PL) spectra of ZnO:Mn thin films with various Mn concentrations.

(V_{Zn}) level [43]. Generally, the visible emission band of ZnO contains green and yellow emissions attributed to the single ionized oxygen vacancy (V_O^+) and the single negatively charged interstitial oxygen ion (O_i^-) [44]. The corresponding emission peaks are shown in figure 6. Furthermore, a broad emission peak around 580 nm is dominant for all samples. This may be ascribed to the deep level emission (DLE) luminescence bands. The DLE band is attributed to the defect states (acceptors) within the band gap of ZnO nanostructured thin films [45].

4. Conclusion

Undoped and Mn-doped nanostructured ZnO thin films with different Mn doping concentrations were successfully prepared using sol-gel dip-coating technique. At lower concentration of Mn doping, the X-ray diffraction pattern showed that the ZnO thin films possess the hexagonal wurtzite structure. With increasing Mn concentration, it was found that the crystalline structure changed and new phases linked to MnO_2 and Mn_3O_4 appeared at 12 wt% of Mn content. SEM images revealed reduction of granular size with increase in Mn doping concentration. The optical transmittance of the prepared thin films showed that the films are transparent in the visible region of the spectrum and the transparency increases steadily to 89% for 3 wt% of Mn concentration and then decreases to 84% for 12 wt% of Mn concentration. Upon increasing the Mn concentration, the optical band gap of the films decreased from 3.89 to 3.15 eV. The PL spectra of the present

nanocrystalline ZnO:Mn thin films showed the presence of several emission peaks pertinent to free excitation transitions, interstitial Zn, local zinc vacancy, single ionized oxygen vacancy, and deep level emissions.

References

[1] A Abdolahzadeh Ziabari and F E Ghodsi, *Sol. Energy Mater. Sol. Cells* **105**, 249 (2012)
[2] A Abdolahzadeh Ziabari and F E Ghodsi, *J. Mater. Sci: Mater. Electron.* **23**, 1628 (2012)
[3] N Karar, F Singh and B R Mehta, *J. Appl. Phys.* **95**, 656 (2004)
[4] A Abdolahzadeh Ziabari and F E Ghodsi, *Thin Solid Films* **520**, 1228 (2011)
[5] A Abdolahzadeh Ziabari and S M Rozati, *Physica B* **407**, 4512 (2012)
[6] J B Lee, M H Lee and C K Park, *Thin Solid Films* **447**, 296 (2004)
[7] E Y M Lee, N Tran, J Russell and R N Lamb, *J. Appl. Phys.* **92**, 2996 (2002)
[8] M H Huang, S Mao, H Feick, H Yan, Y Wu, H Kind, E Weber, R Russo and P Yang, *Science* **292**, 1897 (2001)
[9] C J Lee, T J Lee, S C Lyu, Y Zhang, H Ruh and H J Lee, *Appl. Phys. Lett.* **81**, 3648 (2002)
[10] K Keis, E Magnusson, H Lindstrom, S E Lindquist and A Hagfeldt, *Sol. Energy Mater. Sol. Cells* **73**, 51 (2002)
[11] Y Hu, X Zhou, Q Han, Q Cao and Y Huang, *Mater. Sci. Eng. B* **99**, 41 (2003)
[12] E S Shim, H S Kang and J S Kang, *Appl Surf. Sci.* **186**, 474 (2002)
[13] P Nunes, D Costa and E Fortunato, *Vacuum* **64**, 293 (2002)
[14] Y Kashiwaba, F Katahira and K Haga, *J. Crystal Growth* **221**, 431 (2000)
[15] K Ogata, K Sakurai and S Fujita, *J. Crystal Growth* **214**, 312 (2000)
[16] D F Paraguay, L W Estrada and N D R Acosta, *Thin Solid Films* **350**, 192 (1999)
[17] M Nirmala and A Anukaliani, *Photon. Lett. Pol.* **2**, 189 (2010)
[18] S Suwanboon, T Ratana and T Ratana, *Walailak J. Sci. Tech.* **4**, 111 (2007)
[19] A Abdolahzadeh Ziabari and F E Ghodsi, *J. Alloys Compounds* **509**, 8748 (2011)
[20] J H Lee, K H Ko and B O Park, *J. Crystal Growth* **247**, 119 (2003)
[21] K Y Cheong, N Muti and S R Ramanan, *Thin Solid Films* **410**, 142 (2002)
[22] J Liu, W Weng and W Ding, *Surf. Coat. Technol.* **198**, 274 (2005)
[23] S W Jung, S J An and G C Yi, *Appl. Phys. Lett.* **80**, 4561 (2002)
[24] J Alaria, P Turek and M Bernard, *Chem. Phys. Lett.* **415**, 337 (2005)
[25] E G Birgin, I Chambouleyron and J M Martínez, *J. Comput. Phys.* **151**, 862 (1999)
[26] X Wang, X Wang, W Huang, P J Sebastian and S Gamboa, *J. Power Sources* **140**, 211 (2005)
[27] K J Kim and Y R Park, *J. Crystal Growth* **270**, 162 (2004)
[28] B D Cullity, *Elements of X-ray diffraction*, 2nd edn (Addison-Wesley, London, 1978)
[29] N Shakti, *Appl. Phys. Res.* **12**, 1530 (2010)
[30] G Srinivasan and J Kumar, *J. Crystal Growth* **310**, 1841 (2008)
[31] W Chen, J Wang and M Wang, *Vacuum* **81**, 894 (2007)
[32] S Bandyopadhyay, G K Paul, R Roy, S K Sen and S Sen, *Mater. Chem. Phys.* **74**, 83 (2002)
[33] S Senthilkumaar, K Rajendran, S Banerjee, T K Chini and V Sengodan, *Mater. Sci. Semicond. Process* **11**, 6 (2008)
[34] R N Gayen, K Sarkar, S Hussain, R Bhar and A K Pal, *Indian J. Pure Appl. Phys.* **49**, 470 (2011)
[35] A Abdolahzadeh Ziabari *et al*, *Surf. Coat. Technol.* **213**, 15 (2012)
[36] L Vina and M Cardona, *Phys. Rev. B* **29**, 12 (1984)
[37] R A Abram, G J Rees and B L H Wilson, *Adv. Phys.* **27**, 799 (1978)
[38] E F Schubert, *Doping in III–V semiconductors* (Cambridge University Press, England, 1993) p. 49

[39] W Xu, X Meng, W Ji, P Jing, J Zheng, X Liu, J Zhao and H Li, *Chem. Phys. Lett.* **532**, 72 (2012)
[40] S Ilican, Y Caglar, M Caglar, F Yakuphanoglu and J Cui, *Physica E* **41**, 96 (2008)
[41] Z Fang, Y Wang, D Xu, Y Tan and X Liu, *Opt. Mater.* **26**, 239 (2004)
[42] V S Khomchenko, T G Kryshtab, A K Savin, L V Zavyalova, N N Roshchina, V E Rodionov, O S Lytvyn, V I Kushnirenko, V B Khachatryan and J A Andraca-Adame, *Superlatt. Microstruct.* **42**, 94 (2007)
[43] U Ilyas, R S Rawat, T L Tan, P Lee, R Chen, H D Sun, L Fengji and S Zhang, *J. Appl. Phys.* **111**, 033503 (2012)
[44] X L Wu, G G Siu, C L Fu and H C Ong, *Appl. Phys. Lett.* **78**, 2285 (2001)
[45] U Ilyas, R S Rawat, T L Tan, P Lee, R Chen, H D Sun, F Li and S Zhang, *J. Appl. Phys.* **110**, 093522 (2011)